

## Chapter 2

# Models and Methods

**Abstract** This chapter is devoted to introduce the models and methods we employed in this thesis. We consider Ising-spin Kondo lattice models on frustrated lattices, such as triangular, kagome, and pyrochlore lattices. A strong coupling limit of the Kondo lattice model, double-exchange model, is also introduced. The magnetic and transport properties of these models are numerically studied by using Monte Carlo simulations and variational calculation. Details of these methods are also explained in this chapter. In addition to the numerical calculations on Kondo lattice models, a perturbation approach for deducing the effective spin-spin interactions in the double-exchange models are also explained.

## 2.1 Ising-Spin Kondo Lattice Model

### 2.1.1 Kondo Lattice Model on Frustrated Lattices

To explore the novel magnetic and transport phenomena that emerge from the competition and/or cooperation of spin-charge coupling and geometrical frustration, we here consider a simple model with these aspects, the Ising-spin Kondo lattice model on geometrically frustrated lattices. The Hamiltonian is given by

$$H = -t \sum_{\langle i,j \rangle, \sigma} (c_{i\sigma}^\dagger c_{j\sigma} + \text{H.c.}) - J \sum_i \mathbf{S}_i \cdot \hat{\sigma}_i - \sum_i \mathbf{S}_i \cdot \mathbf{h}. \quad (2.1)$$

The first term represents hopping of itinerant electrons, where  $c_{i\sigma}$  ( $c_{i\sigma}^\dagger$ ) is the annihilation (creation) operator of an itinerant electron with spin  $\sigma = \uparrow, \downarrow$  at  $i$ th site, and  $t$  is the transfer integral. The sum  $\langle i, j \rangle$  is taken over NN sites. The second term is the onsite interaction between localized spins and itinerant electrons, where  $J$  is the coupling constant (the sign of  $J$  does not matter in the present model),

$$\hat{\sigma}_i = \sum_{\alpha, \beta} c_{i,\alpha}^\dagger \boldsymbol{\sigma}_{\alpha\beta} c_{i\beta} \quad (2.2)$$

represents the localized Ising spin at  $i$ th site ( $|\mathbf{S}_i| = 1$ ); and  $\sigma_{\alpha\beta}$  is the vector of Pauli matrices. As we will see in the following sections, along with the models with collinear Ising spins, we also consider the models with different anisotropy axes depending on the sublattices. Hence, the localized spins are denoted by vectors  $\mathbf{S}_i = (S_i^x, S_i^y, S_i^z)$ , where  $S_i^\gamma$  ( $\gamma = x, y, z$ ) is the  $\gamma$  component of the  $i$ th spin. In some sections, we also consider the effect of external magnetic field  $\mathbf{h}$ . The third term in Eq. (2.1) describes the external magnetic field acting on the localized moments. For simplicity, we ignore the effect of magnetic field on the itinerant electrons. This corresponds to the limit in which the localized spins have infinitely large magnetic moments; such a limit is reasonably justified in some realistic situation, such as the rare-earth and transition-metal compounds discussed in the introduction, as they are expected to have large magnetic moments.

### 2.1.2 Strong Coupling Limit

In Chaps. 6 and 8, we consider the strong- $J$  limit of Eq. (2.1). In this limit, the spin of each itinerant electron is perfectly polarized along the direction of the localized moment at each site. As a consequence, the spin indices for itinerant electrons are projected out. Instead, the spin-charge coupling modifies the hoppings of itinerant electrons [1, 5]; this limit is known as the double-exchange limit (see Sect. 1.2.2). The Hamiltonian in this limit is given by

$$H = - \sum_{\langle i, j \rangle} (t_{ij} \tilde{c}_i^\dagger \tilde{c}_j + \text{H.c.}) - \sum_i \mathbf{h} \cdot \mathbf{S}_i, \quad (2.3)$$

where

$$t_{ij} = t \left( \cos \frac{\theta_i}{2} \cos \frac{\theta_j}{2} + \sin \frac{\theta_i}{2} \sin \frac{\theta_j}{2} e^{-i(\varphi_i - \varphi_j)} \right) \quad (2.4)$$

is the hopping matrix element between  $i$ th and  $j$ th site modulated by the relative angle between the  $\mathbf{S}_i$  and  $\mathbf{S}_j$ ;  $(\theta_i, \varphi_i)$  are the polar coordinates for the localized moment at  $i$ th site;

$$\mathbf{S}_i = (S_i^x, S_i^y, S_i^z) = S(\sin \theta_i \cos \varphi_i, \sin \theta_i \sin \varphi_i, \cos \theta_i). \quad (2.5)$$

## 2.2 Monte Carlo Simulation

To numerically analyze the models in Eqs. (2.1) and (2.3), we performed an unbiased Monte Carlo (MC) simulation which has been widely used to study similar models [2–4]. The method is generally applicable to the fermion models coupled to classical fields whose Hamiltonian is given in a quadratic form in terms of the fermion

operators. To be specific, however, we particularly consider the case of itinerant electrons coupled to localized spins.

In general, the partition function for such a model is obtained by taking two traces; one is over the classical fields and the other over the fermion degree of freedom. For the present model in Eq. (2.1), the partition function is written as

$$Z = \text{Tr}_{\{\mathbf{S}_i\}} \text{Tr}_{\{c_{i\sigma}, c_{i\sigma}^\dagger\}} \exp \left[ -\beta \left( H(\{\mathbf{S}_i\}) - \mu \hat{N}_c \right) \right], \quad (2.6)$$

where  $\text{Tr}_{\{\mathbf{S}_i\}}$  and  $\text{Tr}_{\{c_{i\sigma}, c_{i\sigma}^\dagger\}}$  are the traces over the Ising spins and the electron operators, respectively, and  $H(\{\mathbf{S}_i\})$  is a one-particle Hamiltonian matrix in Eq. (2.1) defined for a given Ising spin configuration  $\{\mathbf{S}_i\} = (\mathbf{S}_1, \mathbf{S}_2, \dots, \mathbf{S}_N)$  where  $N$  is the number of the sites;  $\beta = 1/T$  is inverse temperature,  $\mu$  is the chemical potential, and  $\hat{N}_c = \sum_{i\sigma} c_{i\sigma}^\dagger c_{i\sigma}$ . The former trace can be calculated by classical MC sampling of the spin configurations  $\{\mathbf{S}_i\}$  with the Boltzmann weight

$$P(\{\mathbf{S}_i\}) = \frac{1}{Z} \exp [-S_{\text{eff}}(\{\mathbf{S}_i\})], \quad (2.7)$$

where the effective action is given by the latter trace in the form

$$S_{\text{eff}}(\{\mathbf{S}_i\}) = -\log \left( \text{Tr}_{\{c_{i\sigma}, c_{i\sigma}^\dagger\}} \exp \left[ -\beta \left( H(\{\mathbf{S}_i\}) - \mu \hat{N}_c \right) \right] \right). \quad (2.8)$$

A straightforward method to calculate the effective action is the numerical diagonalization of  $H(\{\mathbf{S}_i\})$  [4]. By using the one-particle eigenvalues for  $H(\{\mathbf{S}_i\})$ ,  $\{\varepsilon_\nu(\{\mathbf{S}_i\})\}$ , the effective action is calculated by

$$S_{\text{eff}}(\{\mathbf{S}_i\}) = \sum_{\nu=1}^{N_{\text{dim}}} F[\varepsilon_\nu(\{\mathbf{S}_i\})], \quad (2.9)$$

where  $F[x] = -\log [1 + \exp \{-\beta(x - \mu)\}]$  and  $N_{\text{dim}}$  is the dimension of the Hamiltonian ( $N_{\text{dim}} = 2N$  in the present case).

## 2.3 Polynomial Expansion Method

In the polynomial-expansion Monte Carlo (PEMC) method, the sum over the eigenstates is replaced by the integration over the density of states (DOS), and the integral is evaluated by using the polynomial expansion technique [3];

$$S_{\text{eff}}(\{\mathbf{S}_i\}) = \int d\varepsilon D_{\{\mathbf{S}_i\}}(\varepsilon) F(\varepsilon) = \sum_m \mu_m f_m, \quad (2.10)$$

where  $D_{\{\mathbf{S}_i\}}$  is DOS for itinerant electrons for a spin configuration  $\{\mathbf{S}_i\}$ .

In Eq. (2.10), DOS and  $F$  are expanded by Chebyshev polynomials as

$$\mu_m = \int_{-1}^1 dx T_m(x) \tilde{D}_{\{\mathbf{S}_i\}}(x) = \text{Tr } T_m[H(\{\mathbf{S}_i\})], \quad (2.11)$$

$$f_m = \frac{-1}{\alpha_m} \int_{-1}^1 \frac{dx}{\pi \sqrt{1-x^2}} T_m(x) F(x), \quad (2.12)$$

where  $\alpha_m = 1$  for  $m = 0$  and otherwise  $1/2$ . Here, DOS is renormalized so that the entire spectrum fits into the range of  $x = [-1, 1]$ ;

$$\tilde{D}_{\{\mathbf{S}_i\}}(x) = a D_{\{\mathbf{S}_i\}}(ax + b). \quad (2.13)$$

where  $a = (\varepsilon_{\text{top}} - \varepsilon_{\text{btm}})/2$  and  $b = (\varepsilon_{\text{top}} + \varepsilon_{\text{btm}})/2$ . In the case of a pyrochlore lattice with finite  $J/t$ , we take  $\varepsilon_{\text{top}} = 2t + J + 1$  and  $\varepsilon_{\text{btm}} = -6t - J - 1$  (we afford a margin of 1 for both  $\varepsilon_{\text{top}}$  and  $\varepsilon_{\text{btm}}$ ). On the other hand, in the case of  $J/t \rightarrow \infty$  limit, we take  $\varepsilon_{\text{top}} = 2t + 1$  and  $\varepsilon_{\text{btm}} = -6t - 1$ . In Eqs. (2.11) and (2.12), the Chebyshev polynomials  $T_m$  are calculated by using the recursion relation in the form

$$T_m(x) = 2xT_{m-1}(x) - T_{m-2}(x), \quad (2.14)$$

with

$$T_0(x) = 1, \quad T_1(x) = x. \quad (2.15)$$

In the MC update, we choose a single spin (or several spins) randomly and flip it (or them) by probability  $p$ , which is given by the standard Metropolis algorithm, i.e.,

$$p = \frac{\exp[-\beta S_{\text{eff}}(\{\mathbf{S}_i\}^f)]}{\exp[-\beta S_{\text{eff}}(\{\mathbf{S}_i\}^i)]}. \quad (2.16)$$

Here,  $\{\mathbf{S}_i\}^i$  is the initial spin configuration and  $\{\mathbf{S}_i\}^f$  is the flipped configuration.

When evaluating  $S_{\text{eff}}(\{\mathbf{S}_i\}^i)$  and  $S_{\text{eff}}(\{\mathbf{S}_i\}^f)$  in PEMC, the Chebyshev moments  $\mu_m$  are evaluated by calculating the Chebyshev polynomials of the Hamiltonian matrix recursively. For the sparse Hamiltonian matrix, the calculation amount of  $\mu_m$  is  $O(N^2 \log N)$ , as the necessary order of polynomials scales as  $\log N$ . In one MC step, we go through the above process  $N$  times recursively. Hence, the total cost for one MC step in PEMC is  $O(N^3 \log N)$  [3], which is reduced from  $O(N^4)$  in the Monte Carlo method using the numerical diagonalization.

### 2.3.1 Truncation Algorithm

An efficient way to further reduce the calculation amount is to employ a truncation algorithm [2]. In the truncation procedure, a real-space basis  $\mathbf{e}_j(k) = \delta_{j,k}$  is chosen

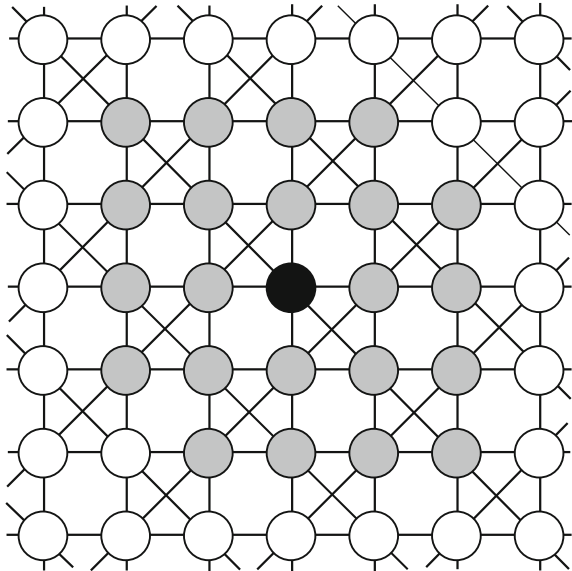
for the trace in Eq. (2.11), where  $k$  is a site index. A new vector  $\mathbf{v}_j^{(m)}$  is generated by multiplying the unit vector by the  $m$ th Chebyshev polynomial of the Hamiltonian, as

$$\mathbf{v}_j^{(m)} = T_m[H(\{\mathbf{S}_i\})]\mathbf{e}_j \equiv \sum_k v_{j,k}^{(m)} \mathbf{e}_k. \quad (2.17)$$

If the hopping term in the Hamiltonian is limited to nearest-neighbor sites as in Eq. (2.1), the coefficient  $v_{j,k}^{(m)}$  takes a nonzero value only if  $\|j - k\| \leq m$  is satisfied, where  $\|j - k\|$  is the Manhattan distance between two sites  $j$  and  $k$ . Furthermore, the coefficient usually becomes small quickly as the Manhattan distance increases. Hence, the vector elements of  $\mathbf{v}_j^{(m)}$  with such small amplitudes can be neglected in the calculation of the moment  $\mu_m$ . In particular, the truncation was done by introducing a threshold for the amplitude of vector elements,  $\epsilon$ , and ignoring the small elements which satisfy  $|v_{j,k}^{(m)}| < \epsilon$  in the calculation of Eq. (2.17) [2]. A similar truncation was also introduced in the trace operation to calculate the effective action  $S_{\text{eff}}(\{\mathbf{S}_i\})$ . This algorithm further reduces the total cost of one MC update to  $O(N)$  [2].

In this study, we considered a similar but slightly different truncation algorithm. We carry out the truncation by a real-space distance, not by a magnitude of the vector element in the original scheme; namely, we set a truncation distance  $d$  and ignore all contributions out of the range of the Manhattan distance  $d$  from a flipped spin. An example of sites within Manhattan distance  $d \leq 2$  is shown in Fig. 2.1 for checkerboard lattice. In the present method, the list of sites to be considered in the calculation is known in advance and unchanged throughout the MC simulation. On the other hand, in the previous method, the list needs to be updated by looking at the

**Fig. 2.1** Schematic picture of the real-space truncation. The figure shows a projection of the pyrochlore lattice onto a  $\{001\}$  plane, and circles represent the lattice sites. The black circle in the center represents the site with flipped spin. Gray circles indicate the sites within the range of the truncation distance  $d$ . The picture shows an example of  $d = 2$



elements of  $\mathbf{v}_j^{(m)}$  in each MC step. Therefore, the present algorithm is much simpler than the previous one.

In previous studies, this method was shown to be efficient in reducing the computational costs [2]. The benchmark on the efficiency of this method for the model in Eq. (2.1) is presented in Sect. 9. We, however, found that the truncation method is less efficient for the system sizes that we calculated. Hence, we did not use the truncation method, and instead, used the original PEMC method in Chaps. 7 and 8.

### 2.3.2 Physical Quantities

In this algorithm, the calculation of physical quantities related to the localized spin degrees of freedom (e.g., magnetization and its susceptibility) can be done in the same manner as the classical Monte Carlo method. Formally, it is done by replacing the internal energy with  $S_{\text{eff}}(\{\mathbf{S}_i\})$ ,

$$\langle O_s \rangle = \frac{1}{Z} \text{Tr}_{\{\mathbf{S}_i\}} O_s \exp[-S_{\text{eff}}(\{\mathbf{S}_i\})]. \quad (2.18)$$

Here,  $O_s = O_s(\{\mathbf{S}_i\})$  is a function for a physical quantity related to spins. The susceptibility for  $O_s$ ,  $\chi_{O_s}$ , is calculated from the fluctuation of  $O_s$ ,

$$\chi_{O_s} = \frac{1}{T} (\langle O_s^2 \rangle - \langle O_s \rangle^2). \quad (2.19)$$

When calculating a physical quantity related to electronic degree of freedom, such as internal energy, the calculation should be done by appropriately taking into account of the Fermi distribution function

$$\langle \hat{O}_e \rangle = \frac{1}{Z} \text{Tr}_{\{\mathbf{S}_i\}} O_e(\{\mathbf{S}_i\}) \exp[-S_{\text{eff}}(\{\mathbf{S}_i\})], \quad (2.20)$$

with

$$O_e(\{\mathbf{S}_i\}) = \text{Tr}_{\{c_{i\sigma}, c_{i\sigma}^\dagger\}} \hat{O}_e(\{\mathbf{S}_i\}) \exp(-\beta H). \quad (2.21)$$

Here,  $O_e(\{\mathbf{S}_i\})$  is a physical quantity for itinerant electrons which is given in the quadratic form in terms of  $c_{i\sigma}$ , and  $\text{Tr}_{\{c_{i\sigma}, c_{i\sigma}^\dagger\}}$  is the trace over the electronic degree of freedom.

As numbers of different parameters are used in each chapter, the details of the actual quantities calculated were described in each chapter separately. We also note that we used different notations as defined in each chapter.

### 2.3.3 Conductivity

To investigate the transport properties, we calculated the conductivity by the standard Kubo formula in a similar manner as in Eq. (2.21). For instance, the optical conductivity along the direction  $v$  induced by an electronic field along the direction  $\eta$  was calculated by

$$\sigma_{\eta v}(\omega, T) = -i\text{Tr}_{\{S_i\}} \left[ \sum_{m,n} \frac{f(\varepsilon_n) - f(\varepsilon_m)}{\varepsilon_m - \varepsilon_n} \frac{\langle m | \hat{j}_\eta | n \rangle \langle n | \hat{j}_v | m \rangle}{\omega - \varepsilon_m + \varepsilon_n + i\tau^{-1}} \right], \quad (2.22)$$

where,  $f(\varepsilon)$  is the Fermi distribution function,  $\varepsilon_m$  is the eigenenergy for  $m$ th state of itinerant electrons, and  $\tau$  is the scattering rate. Here,

$$\hat{j}_\eta = -it \sum_{\langle j,k \rangle, \sigma} (\mathbf{n}_\eta \cdot \boldsymbol{\delta}_{j,k}) (c_{k\sigma}^\dagger c_{j\sigma} - c_{j\sigma}^\dagger c_{k\sigma}) \quad (2.23)$$

is a current operator in the  $\eta$  direction ( $\eta$  is assigned for each case below), which is constructed in a standard way from a polarization operator in order to satisfy the continuity equation. Here,  $\mathbf{n}_\eta$  is the unit vector in the  $\eta$  direction and  $\boldsymbol{\delta}_{j,k}$  is the geometrical vector from  $j$ th to  $k$ th site. The sum is taken for all the nearest-neighbor pairs. The details on the parameters we used in the calculations are given in each chapter.

## 2.4 Variational Method

In addition to the MC method introduced in Sects. 2.2 and 2.3, the ground state phase diagrams were studied using a variational method comparing the ground state energy of different magnetically ordered states obtained in the MC simulation.

In the variational calculation, we first calculated the electron density and internal energy for each magnetic orders with varying the chemical potential  $\mu$ . The ground state at different  $\mu$  are obtained by comparing the ground state energy for different magnetic states. The phase diagram with respect to  $\mu$  is then mapped onto the phase diagram with varying  $n$ ; the phase separation between different magnetic states is determined from the jump of  $n$  at the phase boundary. As an example, the variational calculation for the triangular lattice model is presented in Sect. 3.3.4.

## 2.5 Perturbation Method in the Strong Coupling Limit

In the pyrochlore lattice cases in Chaps. 7 and 8, we also derived an effective spin model to analyze the phase diagram. In the weak coupling limit, the perturbation theory in terms of  $J/t$  which leads to the RKKY interaction, is expected to be a

useful approach; the details of this approach is explained in Sect. 1.2.1 and is used in Chap. 7. On the other hand, in the strong coupling limit, we introduced a perturbation theory in terms of the relative angle of the localized moments. In the strong coupling limit, the hopping integrals for itinerant electrons are modulated by the relative angle of localized moments (Eq. (2.4)). For simplicity, we approximate the hopping Eq. (2.4) by its absolute value

$$\tilde{t}_{ij} = |t_{ij}| = t \sqrt{1 + \cos \theta_i \cos \theta_j + \frac{1}{2} \sin \theta_i \sin \theta_j \cos(\varphi_i - \varphi_j)} \quad (2.24)$$

$$= t \cos(\theta_{ij}/2), \quad (2.25)$$

where,  $\theta_{ij}$  is the angle between the  $i$ th and  $j$ th spins.<sup>1</sup> In the current models, as the spins are of Ising type, Eq. (2.25) can be transformed into

$$\tilde{t}_{ij} = t_0 + t_1 \tilde{S}_i \tilde{S}_j \quad (2.26)$$

with

$$t_0 = \frac{1}{2} \left( \cos \frac{\theta_{ij}^0}{2} + \sin \frac{\theta_{ij}^0}{2} \right) \quad (2.27)$$

$$t_1 = \frac{1}{2} \left( \cos \frac{\theta_{ij}^0}{2} - \sin \frac{\theta_{ij}^0}{2} \right), \quad (2.28)$$

where  $\theta_{ij}^0$  is the relative angle between the easy axes of neighboring sites and  $\tilde{S}_i = \pm 1$  is the Ising spin on  $i$ th site projected onto its anisotropy axis. When  $\theta_{ij}^0 = \pi/2$ , then  $t_1 = 0$ ; hence, the orientation of localized Ising moments does not affect itinerant electrons. When  $\theta_{ij}^0 \sim \pi/2$ ,  $t_1$  remains much smaller than  $t_0$ . As the angle between the two nearest-neighbor spins is  $\sim 109^\circ$  for the spin-ice model considered in Chap. 8, and close to  $\pi/2$ , we performed perturbation theory in terms of  $t_1/t_0$ . Essentially, this perturbation expansion corresponds to the perturbation for  $\Delta\theta_{ij}^0 = \pi/2 - \theta_{ij}^0$ .

## References

1. P.W. Anderson, H. Hasegawa, Phys. Rev. **100**, 675 (1955)
2. N. Furukawa, Y. Motome, J. Phys. Soc. Jpn. **73**, 1482 (2004)
3. Y. Motome, N. Furukawa, J. Phys. Soc. Jpn. **68**, 3853 (1999)
4. S. Yunoki, J. Hu, A.L. Malvezzi, A. Moreo, N. Furukawa, E. Dagotto, Phys. Rev. Lett. **80**, 845 (1998)
5. C. Zener, Phys. Rev. **82**, 403 (1951)

---

<sup>1</sup>In principle, the perturbation expansion can also be done by considering the complex hopping. However, for simplicity, we used the approximation in Eq. (2.25).



Magnetism and Transport Phenomena in Spin-Charge  
Coupled Systems on Frustrated Lattices

Ishizuka, H.

2015, XIV, 133 p. 72 illus., 67 illus. in color., Hardcover

ISBN: 978-4-431-55662-6